SIDE WIND EFFECT ON THE SMALL BUCKET CRANE IN CASE OF ELEVATED BUCKET: MODELLING AND NUMERICAL ANALYSIS

Ilir DOÇI[1], Ferit IDRIZI [2*], Naser LAJQI[3]

The paper examines the impact of the wind blowing on the side of the specific type of crane known as Bucket crane. Because it blows perpendicular to the crane's left or right side, it is referred to as a side wind or a cross wind. The study is done for the case of work operation when the bucket, or platform, is positioned 13 meters from the ground. In this elevated position, the blowing of strong wind can pose high risk for the stability and overturning. Comsol Multiphysics software is used to model the crane, design the virtual wind tunnel around the crane, and carry CFD numerical analysis. The virtual wind tunnel is designed with the freestream velocity of the side wind on the side of the crane. Laminar and turbulent flow are the two wind flow regimes that are examined. Results of the side wind impacts, including wind pressure, wind stream form and flow, velocity field, velocity vortex, and stress on the crane, will be presented. The study falls under the domains of crane safety, CFD numerical analysis, and mobile crane aerodynamics.

Keywords: Bucket crane, side wind, CFD analysis, laminar flow, turbulent flow, crane modelling, crane safety

1. Introduction

A bucket crane is a small truck-crane that is used to lift workers using a platform called a "bucket," for maintenance of streetlights, construction works, tree care, and occasionally for material lifting. (Fig.1). Other names for it include platform boom crane, aerial platform truck, and bucket truck. It is frequently referred to as a truck in literature and is under the category of mobile cranes. It operates in an open area and is regularly hit by wind, which could pose a safety risk if workers are on the platform at a particular height while doing their jobs. We used a small bucket crane [1] from a local business that performs this kind of work in Prishtina City, the capital of Kosovo, as an example for the analysis in this research. The crane stands motionless while the work is being done. The

[1] Professor, Department of Engineering design and vehicles, University of Prishtina, Faculty of Mechanical Engineering, Kosovo, e-mail: ilir.doci@uni-pr.edu .
[2]* Professor, Department of Industrial engineering, University of Prishtina, Faculty of Mechanical Engineering, Kosovo, e-mail: ferit.idrizi@uni-pr.edu (Corresponding Author).
[3] Professor, Department of Engineering design and vehicles, University of Prishtina, Faculty of Mechanical Engineering, Kosovo, e-mail: naser.lajqi@uni-pr.edu .

crane's left or right side is struck by the side wind, which is determined by its velocity and direction. It has a high velocity (up to 60 km/h), frequently fluctuates in flow, and can change course [2], [3]. Excessive wind can cause oscillations and swinging, which can be dangerous for both the workers' and the crane's safety [4], [5]. In the field of mobile crane dynamics, analyzing the impact of wind on mobile cranes is a crucial topic [6], [7].

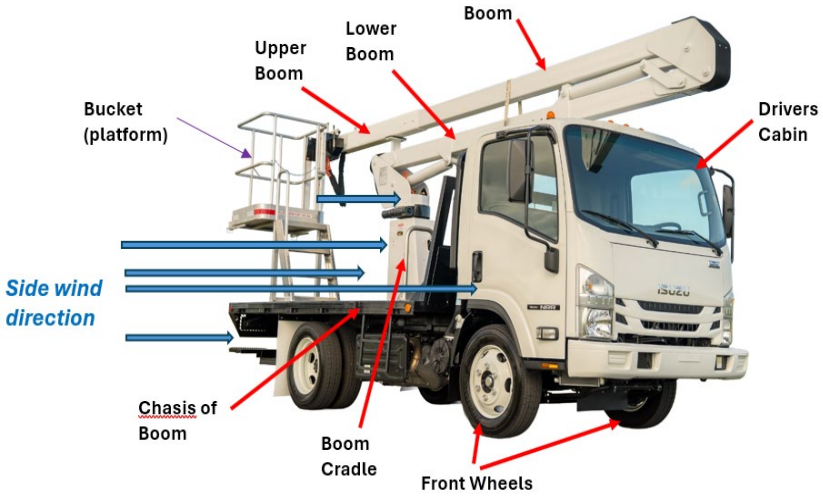

Fig.1. Bucket Crane with its main parts and the direction of the Side wind

Main technical features of the Bucket Crane are (Fig.1): Gross Vehicle weight W = 8845 kg, Bucket maximal carrying mass Q =160 kg, Vertical extension of the bucket H= 13 m, Horizontal extension of the bucket H= 7 m, Wheelbase/No.of axles L = 3360 mm / 2, Motor power 88 kW, 540 degree Boom rotation [1], [8].

2. Literature Review

The literature review includes contributions and articles by authors on the wind's influence on similar types of trucks and cranes, as well as modeling and CFD numerical analysis on the subject.

J. Huang et al. [2] present a combined command shaping and feedback control architecture for a boom crane model subjected to wind disturbances. They suggest an input shaper to eliminate payload oscillation caused by human-operator commands, while the feedback controller mitigates the effects of wind gusts. *I. Doçi et al*. [3] developed a 3D model of a construction crane and applied wind force to the crane's side to study stability and oscillation control. They did this using SimWise4D software. *D. Cekus et al.* [7] proposed a dynamic model of the mobile crane that incorporates the effect of wind pressure during load transfer and

positioning. They developed an algorithm and computational software for assessing dynamic phenomena during both work cycles and free movement of the load. *X. Zhang* [11] proposed a probabilistic method for studying vehicle crosswind stability as well as nonstationary aspects for risk assessment under strong crosswind conditions. He developed a stochastic gust model with non-stationary wind turbulence.

F. A. Monteiro et al. [12] provide a numerical analysis of how wind affects loads hoisted by offshore cranes. They provide an analysis approach in which the platform module's drag coefficients are computed using CFD and the pendulum-like displacement is calculated using a finite difference scheme. *I. Doçi et al*. [13] developed the 3D model of the heavy transportation truck and used CFD to study the impacts of the wind blowing on the backside of the truck while moving forward. *F. Frunzulica et al.* [14] present the staged creation of a simpler vehicle model using CFD for aerodynamic design. They additionally develop a fully three-dimensional region of separated flow that can show the physics of flow.

A. Alonso-Estébanez et al. [15] using a numerical technique called Large Eddy Simulation (LES), show how different testing truck infrastructure features affect vehicle aerodynamic properties when crosswind is present. *M. Augustyn et al* [16] calculate the critical wind speed that leads to the overturning of the fast-erecting crane structure. They perform the numerical analysis of the simplified model of the crane on a real-scale basis. They use the turbulent flow k-ε model. *Labesh Kumar* [17] outlined the process for lowering drag in big trucks to reduce fuel consumption. Using the CATIA software, he created various vehicle geometries and shape changes and ran simulations. *S. Walczak et al.* [18] described the method of determining aerodynamic forces acting on a vehicle going through the region of sadden cross wind using the simulation program CarDyn developed by the author.

Most of the articles use the technique, which involves developing a 3D model of a crane or truck, performing a CFD study, and frequently running simulations using the appropriate software to determine how wind affects the structure of the vehicle. The authors emphasize the significance of proper 3D modeling, organizing the CFD study in advance, and determining relevant resultant parameters.

There are several publications that discuss how wind affects trucks and cranes, but it is hard to find one that examines the impact of side winds on this kind of crane. This served as the motivation for the creation of this study. Investigating workplace safety risks while being hit by strong side winds served as another incentive. This paper contributes significantly to this topic. The 3D model developed is accurately comprehensive in the typical working position and with the virtual tunnel carefully designed to accurately represent the side wind flow in, out and around the crane. Since side wind influence on the bucket crane

has not been thoroughly examined, it was difficult to determine the key resultant features that would provide a better comprehension of the event. Study of two main flow regimes: Laminar flow and turbulent flow ads to the quality of analysis. When there is wind, laminar flow occurs for the most of the year. High-velocity turbulent flow is uncommon but should always be taken into account. Additionally, the study methodology that has been described can be further applied to cranes and trucks of a similar type.

3. Designing the 3D model of the Bucket Crane

The 3D model of the crane is designed to represent the main work operation, which is when the bucket is elevated in the certain height. The Boom is raised and the bucket is at the height aprox. 13 m from the ground (Fig.2). This is maximal lifting position of the bucket [8]. The lifting height is also compatible for the height of street lamps that reach up to 12 m [19]. The 3D model has 18 main parts designed and interconnected.

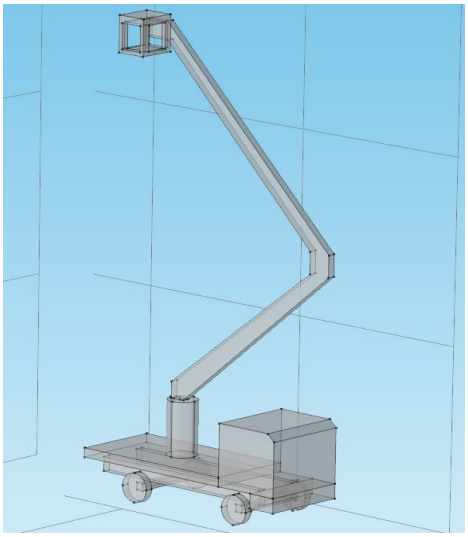

Fig.2. View of the 3D Model of the crane with its main parts, without the Wind tunnel

Besides the Crane model, the Wind tunnel (virtual) is designed with its walls around the Crane (Fig.3). It will be added to define the Side wind blowing on the right side of the Crane. Dimensions of the virtual wind tunnel are Height 18 m, Length 12 m, Depth 12 m (Fig.3). For comparison, dimensions of the bucket crane, are Height 13 m, Length 6.5 m, Depth 2.3 m. In the Inlet flow surface of the wind tunnel is defined the wind entry flow. If there is an inlet surface, there ought to be an outlet surface as well, possibly with different boundary parameters. In the outlet flow surface is defined the exit stream of the wind. The wind tunnel

is longer in the outlet flow from the crane for about 1 m compared to the inlet flow. Other surfaces: front surface, rear surface, and upper surface are designed as a freestream air motion. The bottom of the virtual tunnel is designed as a flat surface, representing the road where crane stands. It has Symmetry boundary condition, which prescribes no penetration and vanishing shear stresses.

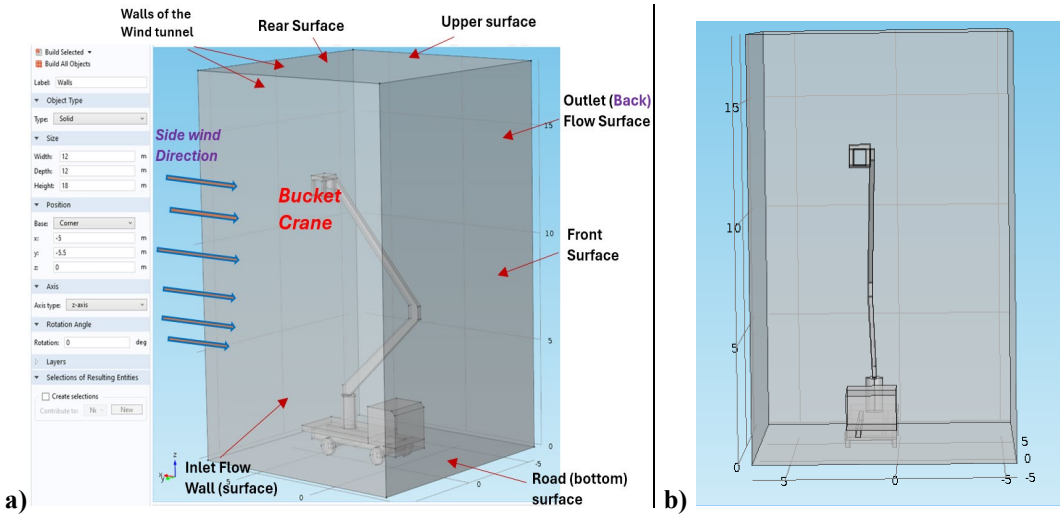

Fig.3. a) Parts of the virtual Wind tunnel and its dimensions; b) Front view of the tunnel and crane

4. Computational Fluid Dynamics parameters for the model design

The input parameters important to define the study are from the field of CFD analysis. Wind velocity is one of the main parameters in the model. It is defined in the Inlet Wall of the Virtual tunnel, and it blows in streams perpendicular to the Right Side of the Bucket Crane (Fig.3). The intensity of the Side wind is defined with the velocity, which is measured experimentally in the city of Prishtina [3], [13]. According to the measurements, the highest value of the wind velocity, in form of the wind gust, is $v_{wg} = 58.74\ km/h = 16.31\ m/s$. Based on the literature [20], [21] this is considered a high wind velocity and a risk for crane safety.

For this model, Stationary Study is chosen for analysis. Stationary Study is used when field variables do not change over time, such as in stationary problems [9], [22]. In the fluid flow fields, it is used to compute the steady flow and pressure fields [22]. The air flow, or the Side wind flow in a wind tunnel is of type Single phase flow model [9], [23], which is a flow with only one substance, in this case air. It can have two motion regimes: *laminar flow* and *turbulent flow*. Analysis will be conducted for both regimes. Then, acquired results will be discussed and compared.

Laminar airflow - is a type of air movement when air moves in smooth paths or layers and consistent in velocity and direction. There is no disruption between air layers called "laminae", which are almost parallel in motion [22], [23].

The equations solved by the Laminar Flow interface are the Navier-Stokes equations [10], [23], [25] :

$$\nabla\cdot(\rho\mathbf{u}) = 0 \tag{1}$$

$$\rho(\mathbf{u}\cdot\nabla)\mathbf{u} = \nabla\cdot\left[-p\mathbf{I}+\mu(\nabla\mathbf{u}+(\nabla\mathbf{u})^{T})-\frac{2}{3}\mu(\nabla\cdot\mathbf{u})\mathbf{I}\right]+\mathbf{F} \tag{2}$$

Equation (1) is the *Continuity equation* and represents conservation of mass. Equation (2) is a *Vector equation* that represents conservation of momentum.

Parameters of equations are: **u** is the velocity vector; p is pressure; ρ is the density; ∇ is the divergence; **I** is the identity tensor; μ is the dynamic viscosity; **F** is the volume force vector (N/m^3);

Compressible flow (Ma<0.3) is defined for aerodynamic processes. The value of Mach number (Ma) < 0.3 is the limit value for determining incompressibility of fluids. Reference pressure level is 1 [atm]. The ambient temperature is adopted with value $T = 293.15[K] = 20^{o}\,C$. Initial value of velocity field **u** is set to zero. Initial pressure p is set to zero.

The *Walls* of the Wind tunnel are defined for the Stationary flow, with equation **u** = 0, with *No slip* boundary condition.

For the *Inlet* of the Wind Tunnel, the Boundary condition option is the Velocity. The Normal inflow velocity is specified with equation $\mathbf{u} = -\mathbf{n}U_0$, where **n** is the boundary normal pointing out of the domain and U_0 is the normal inflow speed, in this case $U_0 = 16.31$ m/s.

The Stationary equations for the *Outlet* of the Wind Tunnel are [10], [23]:

$$\left[-p\mathbf{I}+\mu(\nabla\mathbf{u}+(\nabla\mathbf{u})^{T})-\frac{2}{3}\mu(\nabla\cdot\mathbf{u})\mathbf{I}\right]\boldsymbol{n} = -\hat{p}_0\boldsymbol{n} \tag{3}$$

$$-\hat{p}_0 \le p_0 \tag{4}$$

Where $\hat{\mathbf{p}}_0$ – Reference pressure related to value of initial pressure $p_0 = 0$.

The *Suppress backflow* is selected by default. This option adjusts the outlet pressure in order to prevent fluid from entering the domain through the boundary.

The *Symmetry* boundary condition prescribes no penetration and vanishing shear stresses. The boundary condition is a combination of a Dirichlet condition and a Neumann condition. Equations for the *Stationary* flow are [10], [23]:

$$\mathbf{u}\cdot\mathbf{n} = 0 \tag{5}$$

$$\mathbf{K} - (\mathbf{K}\cdot\mathbf{n})\mathbf{n} = 0, \qquad \mathbf{K} = \left[\mu(\nabla\mathbf{u}+(\nabla\mathbf{u})^{T})-\frac{2}{3}\mu(\nabla\cdot\mathbf{u})\mathbf{I}\right]\mathbf{n} \tag{6}$$

Turbulent airflow - known as turbulence, is the case when air layers show irregular movement, air motion is characterized by chaotic changes in pressure and flow velocity, while its overall bulk moves in a specific direction [10], [23]. The flow of wind is usually turbulent, even if the currents are mild. There are several turbulence models in the theory of Fluid Dynamics, which are also offered in the software for analysis*: Algebraic yPlus, L-VEL, k-ε, k-ω, SST, Low Reynolds number k- ε, Spalart-Almaras* [10], [22].

In this study is implemented *Spalart-Almaras* Turbulence model. It is a one-equation turbulence model designed mainly for aerodynamic applications. It is a low Reynolds number model, and does not utilize wall functions [10], [22]. *The Reynolds - averaged Navier-Stokes (RANS)* equations (1) and (2) are used to model and analyze air flow for the turbulent flow [26]. Additionally, Turbulence effects are modeled using the Spalart-Allmaras one-equation model. The model solves for the undamped turbulent kinematic viscosity. The model parameters and formula are rather long, and will not be shown here, but can be found in the reference [28]. In this Turbulence model, values are given for 8 dimensionless parameters: $C_{b1} = 0.1355$, $C_{b2} = 0.622$, $C_{v1} = 7.1$, $\sigma_{\tilde{v}} = 2/3$, $C_{w2} = 0.3$, $C_{w3} = 2$, $K_v = 0.41$, $C_{Rot} = 2$, required for the solution of equations.

Wind velocity is $U_0 = 16.31$ *m/s*, same as per Laminar flow. The objective is to determine the impact difference between a turbulent and a laminar wind stream at the same maximum wind velocity. The value of Undamped turbulent kinematic viscosity v is calculated with the formula $v_0 = 3*spf.nu$, where *spf.nu* is the variable of kinematic viscosity. The ambient temperature is 293.15 [K]. Other input parameters: compressibility, atmospheric pressure level, initial pressure $p_0 = 0$ are the same as in laminar flow.

The *Walls* of the Wind tunnel are defined with *No slip* boundary condition and for the Stationary flow the equations are:

$$\mathbf{u} = 0 \; ; \quad v^t = 0 \; ; \qquad G = 2/I_{ref} \tag{7}$$

where: v - Undamped turbulent kinematic viscosity ; G – Reciprocal wall distance ; I_{ref} - parameter of the wall distance to the objects.

For the *Inlet* of the Wind Tunnel for Turbulent flow, the Boundary condition option is the Velocity. The Normal inflow velocity is specified with equations:

$$\mathbf{u} = -\mathbf{n}U_0 \; ; U_{ref} = U_0 \; ; \qquad v^t = v_0 \; ; \qquad \nabla G \cdot \mathbf{n} = 0 \tag{8}$$

The Stationary equations for the *Outlet* of the Wind Tunnel are same as (3) and (4) with the addition:

$$\nabla v^t \cdot \mathbf{n} = 0 \; ; \qquad \nabla G \cdot \mathbf{n} = 0 \tag{9}$$

For the *Symmetry* boundary, equations for the *Stationary* flow are same as (5) and (6) with the addition of equations (9).

Reynolds number (Re) – Is the parameter used to define the difference between the Laminar and Turbulent flow regimes. It represents the ratio between inertial and viscous forces and is a dimensionless number. For the external flow, which is the case here, a flow is considered laminar if the Reynolds number is up to 5×10^5. A flow is considered turbulent if the Reynolds number is greater than 5×10^6. Values in between $5 \times 10^5 < \mathrm{Re} < 5 \times 10^6$ are considered *Transition regime* from laminar to turbulent [22], [23]. The Fluid Flow interface of the software automatically calculates the local cell Reynolds number *Re* depending on the length scale and velocity scale [10]. It doesn't require input of values for any flow regime. Reynold number will be presented as one of the results and discussed.

5. Defining the models Mesh

The model's geometry is discretized in the mesh of small 2D and 3D simple geometrical elements before the results are processed. [14], [24]. The software automatically generates the mesh. The elements size of the Mesh is important for the accuracy of the solution and interpolation of elements nodes, but also affects the time required to solve the model [10], [13]. The finer size of the elements gives more elements in the mesh, which improves accuracy of the results but can also increase processing time and strain computer hardware. For the current model, we chose the *Coarser* size of the mesh while it gave good results in reasonable time and without processing issues. The type of mesh selected is *Free tetrahedral mesh* (Fig.4). The Mesh size of the model contains 67554 tetrahedral elements, 4276 triangular elements, 950 edge elements, 182 vertex elements. The mesh volume is 2592 m^3. Maximum element size is 1.56 m.

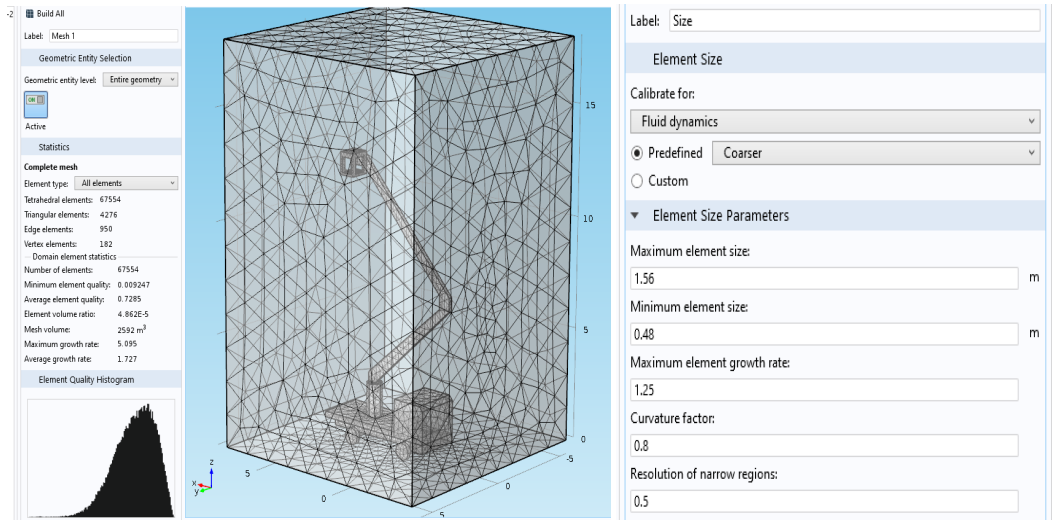

Fig. 4. *Left*- Mesh model of the Bucket Crane and the virtual tunnel with Mesh Statistics; *Right*- Mesh parameters for Coarser density calibrated for Fluid dynamics

6. Results for the Laminar flow regime

For the Laminar flow regime, results are obtained for the main influencing parameters that are *Wind velocity, Vorticity field, Wind Pressure, Stress on the crane, Reynolds number*. Results will be presented in 3D graphs in the form of Surface distribution, Streamlines and Isosurfaces. 2D line graphs will be shown for two selected edges, one in the Bucket and one in the Drivers Cabin for detailed result of the Side wind impact in specific parts of the Crane.

Figure 5 shows the distribution and magnitude of the wind velocity, in the form of isosurfaces on and around the Crane, in two orthogonal views. Darker red colors shows higher magnitude. According to Fig. 5.a, the highest wind velocity values are found behind the driver's cabin, at the back of the crane, and near the bottom of the boom. Based on Fig.5.b, maximal values are more present at the outlet part of the crane. The velocity magnitude can reach up to $U_{max} = 22.5$ *m/s,* although the input velocity is $U_o = 16.31$ *m/s.* This is an increase of 38%. This occurs as a result of the cranes' structure creating additional resistance or drag to the wind blow. Drag is aerodynamic force or resistance that acts opposite to the direction of the wind flow [21], [22]. The wind velocity on the platform (bucket) has a magnitude around $U_{pl} = 21$ *m/s.* In comparison to the boom or drivers cabin, it may be stated that the bucket has a lower wind velocity magnitude. The problem is the high wind speed on the boom, which can cause the entire crane to swing and oscillate excessively and pose a safety risk. [20], [27].

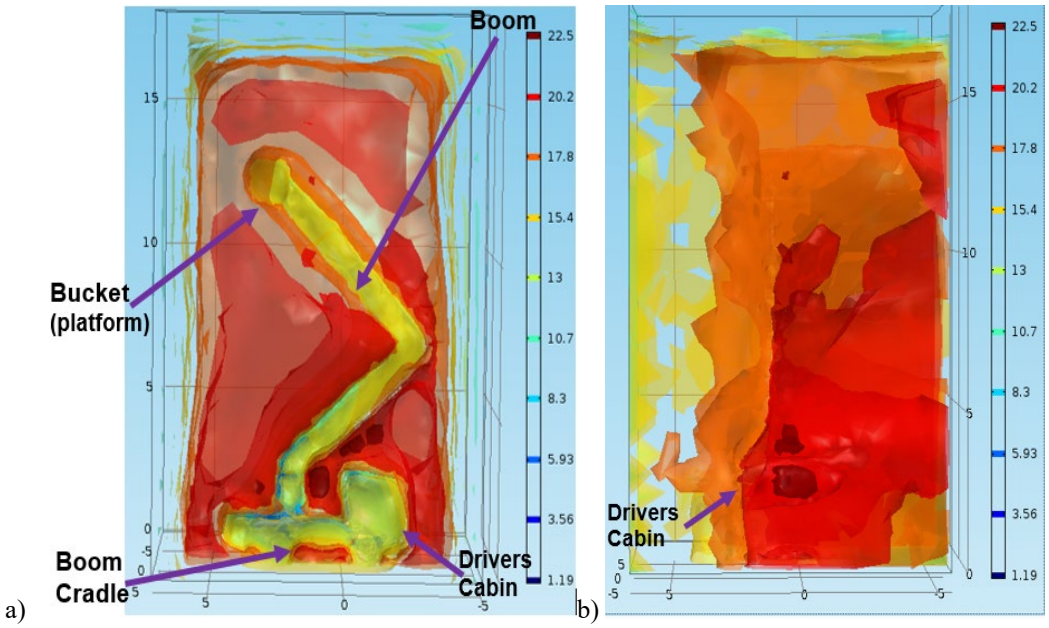

a) b)

Fig. 5. Distribution of the wind velocity and its magnitude around the crane (m/s): a) Right side view, b) Front side view

In the Fig.6 is the 3D graph of the vorticity field around the crane. Vorticity is a measure of rotational motion of the air, with the unit *1/s*, and in this case represents the local spinning motion of the wind around the crane [22]. Vorticity curves with highest density are at the outlet part, in front of the drivers cabin and around the Boom.

In Fig.7 is shown the 3D graph of the pressure distribution on the crane from the wind blow, in the form of isosurfaces, measured in unit *Pa*. Maximal pressure values (orange to red color) are present on the right side of the Drivers cabin, Boom Cradle and below the Crane, with the maximal value $p_{max1} = 263\ [Pa]$.

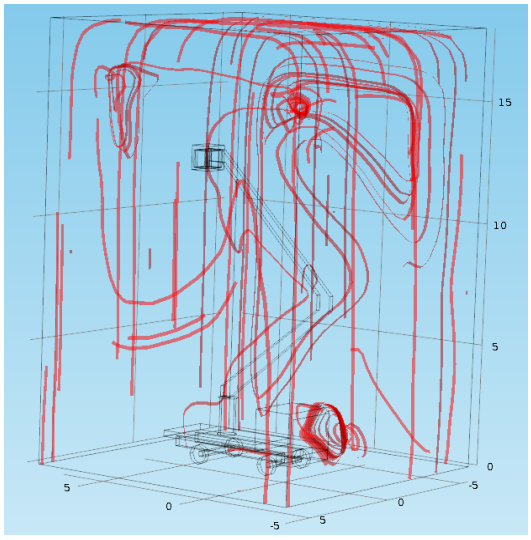

Fig.6. Vorticity field around the crane, for the laminar flow (1/s)

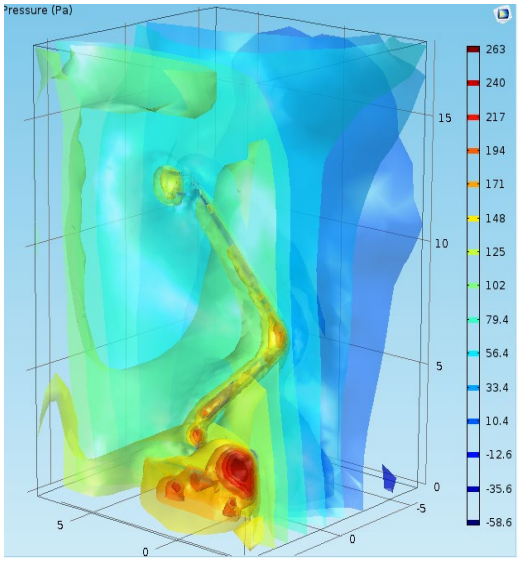

Fig. 7. Pressure on and around the Crane, laminar flow (Pa)

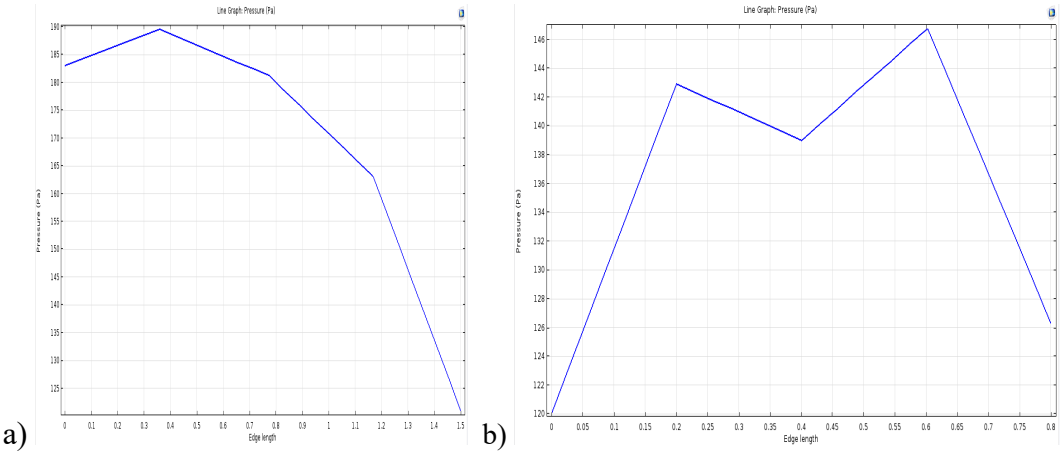

Fig.8. 2D Graph of the pressure on two different edges of the crane: a) vertical edge of the drivers cabin, b) edge of the bucket

In the Fig.8 are 2D graphs representing sample of the wind pressure on two edges of different parts of crane. On Fig.8.a is the pressure on the drivers cabin right edge, with max value $P_{cab} \approx 189\ Pa$. On the Fig.8.b is the pressure on the bucket with max value $P_{bu} \approx 147\ Pa$. The drivers cabin undergoes more pressure, for about 29.2% more than the Bucket.

In Fig. 9 is shown the 3D graph of the Total stress distribution on the crane resulting from the wind blow. The highest values of stress, shown in dark red color, are present in the right of drivers cabin, wheels, and lower parts of the Boom. In these sections, the maximum stress value is around $\sigma_{max} = 260\ Pa$.

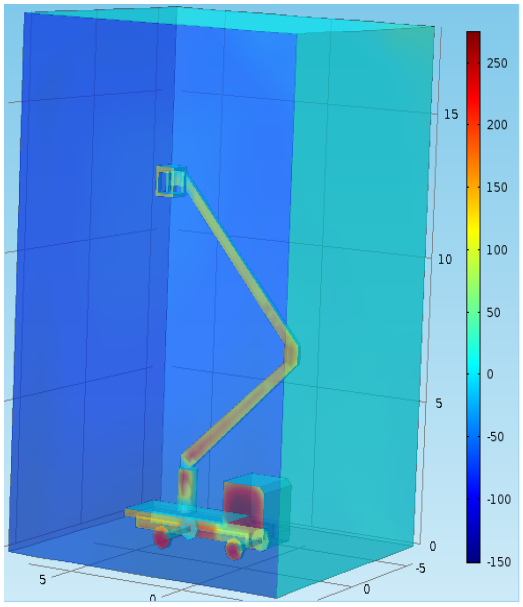

Fig.9. Total stress disstribution on the crane (Pa)

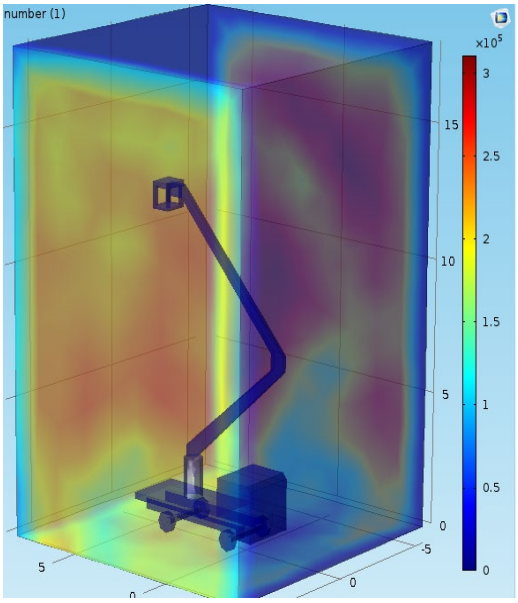

Fig.10. Cell Reynolds number disstribution around the Crane

In Fig. 10 is given the 3D graph of the Cell Reynolds number distribution around the Crane. Based on the results, the maximal value is $R_e = 3.1 \cdot 10^5$, shown in dark red color. Maximal values are present above the crane, around the Boom and Bucket. Based on the numerical values of Reynolds number shown in Chapter 4, the value $R_e = 3.1 \cdot 10^5$ is in the scope of external laminar flow.

7. Results for the Turbulent flow regime

Further will be shown the results for the turbulent flow of the selected model type Spalart-Almaras. In the Fig.11 is the 3D graph of velocity distribution and magnitude in the form of isosurfaces. Maximal values of the velocity are present at the outlet part, around the cabin, lower parts of the Boom and in some parts

below the crane. They reach values up to U_{max} = *23.6 m/s.* This is a matter of concern, while the input wind velocity is U_0 = *16.31 m/s*, so the flow increase around the crane is about 44.7%. Compared to the maximal results for the velocity in the laminar flow, which was *22.5 m/s* (Fig.5), this is an increase for 4.9 %.

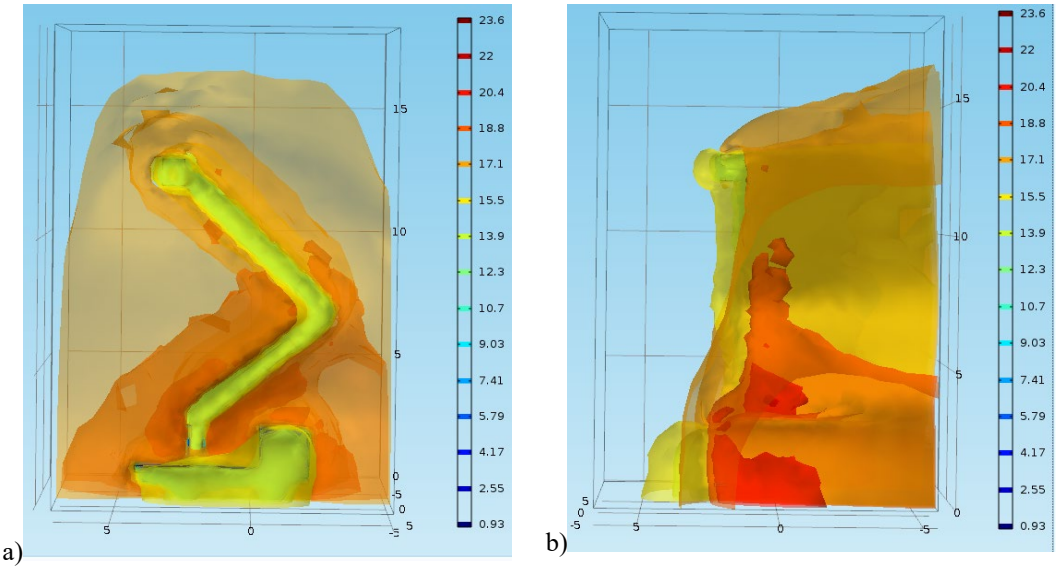

Fig. 11. Distribution of the wind velocity and its magnitude around the crane, for the turbulent flow (m/s): a) Right side view, b) Front side view

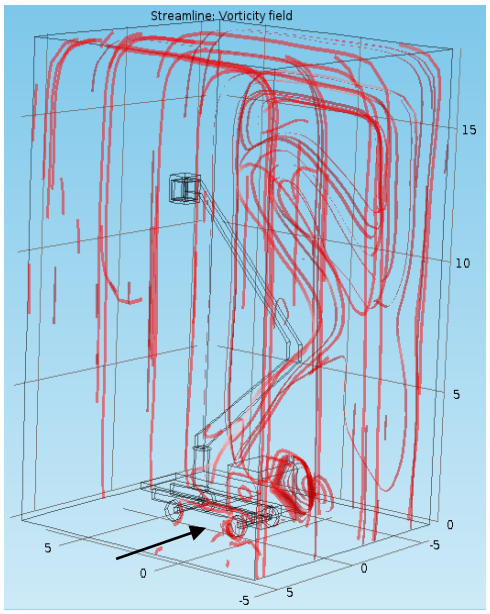

Fig.12. Vorticity field around the crane, for the turbulent flow (1/s)

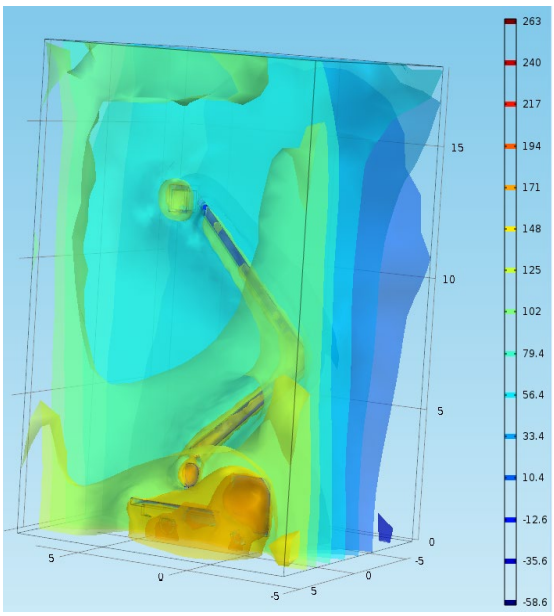

Fig. 13. Pressure on and around the Crane, turbulent flow (Pa)

In Fig.12 is the 3D graph of the vorticity field around the crane for the turbulent flow. Vorticity curves with highest density are present around the drivers cabin and around the Boom. Comparing with the laminar flow (Fig.6) there is an additional vortex on the right side of the crane, shown with arrow and there are more vorticity streams on the outlet surface. We can conclude that, in comparison to the laminar flow, there is more vorticity surrounding the crane in turbulent flow.

In Fig.13 is shown the 3D graph of pressure distribution on the crane for the turbulent flow, in the form of isosurfaces. Comparing the 3D graphs, the form and the magnitude of the pressure are comparable with the laminar flow (Fig.7).

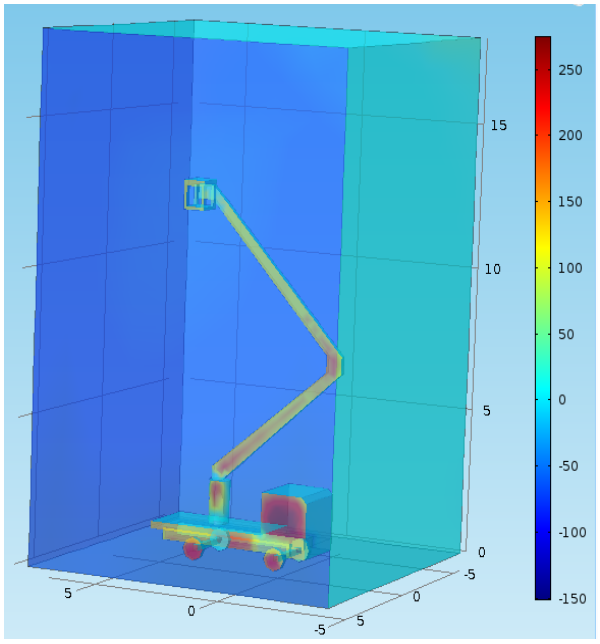

Fig.14. Total stress disstribution on the crane, turbulent flow (Pa)

In Fig. 14 is given the 3D graph of the Total stress distribution on the crane for the turbulent flow. The maximum stress value is around $\sigma_{max} = 260\ Pa$. The form of volume distribution and the magnitude of the Total Stress are comparable with the laminar flow.

In Fig. 15 is the 3D graph of Cell Reynolds number distribution around the crane for the turbulent flow. The form of volume distribution and the magnitude of the Reynolds number are similar with the laminar flow. Higher values are present above the crane, around the Boom and Bucket. Maximal value is around $R_{et} = 3.1 \cdot 10^5$. Although the model selected is turbulent, based on the theoretical values from Chapter 4, the values remain in the scope of external laminar flow.

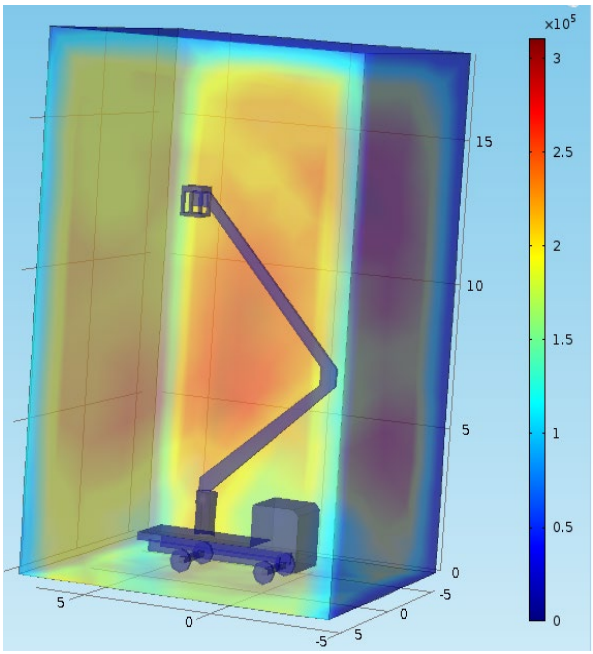

Fig.15. Cell Reynolds number disstribution around the Crane, turbulent flow

The conclusion regarding the turbulent wind flow on the crane is that, in comparison to the laminar flow, the outlet side of the flow is more turbulent and the velocity is larger, but the pressure and stress on the crane are not substantially different.

Furthermore, in order to conduct thorough research, we examined additional turbulence models *k-ε, k-ω, SST* and *Low Reynolds number k-ε* mentioned in Chapter IV that may apply for aerodynamic analysis. The results are comparable to the chosen turbulent model.

8. Grid Independence analysis

To test the accuracy of results, we will carry out Grid Independence analysis. It is a method in CFD analysis to find if there is a difference in calculated results in the cases of different Grid (Mesh) conditions and it is used to test the accuracy of the results and optimizing grid. The main parameter considered is the Mesh density. Mesh can be Finer or Coarser. In our case, the results were calculated for the case of Coarser Mesh (Chap.5). Main Parameters calibrated for Fluid Dynamics analysis are shown in Fig.4, which includes Element Size Parameters: *Maximum element size, Minimum element size, Maximum element growth rate, Resolution of narrow regions*.

For analysis purposes, we will make changes in the *Maximum element size,* which has the current value of 1.56 m (Fig.4) [29]. Instead of numerical value, we

will put variable ***a*** for *Maximum element size* (Fig.16). Then we will assign numerical values for variable ***a*** in an incremental order: 1.3, 1.4, 1.5, 1.6, 1.7, 1.8, 1.9 (Fig.17). These values are around the initial value of 1.56 m. This means that we define 7 different types of Mesh (Grid) that have different density based on 7 different maximum values of their elements.

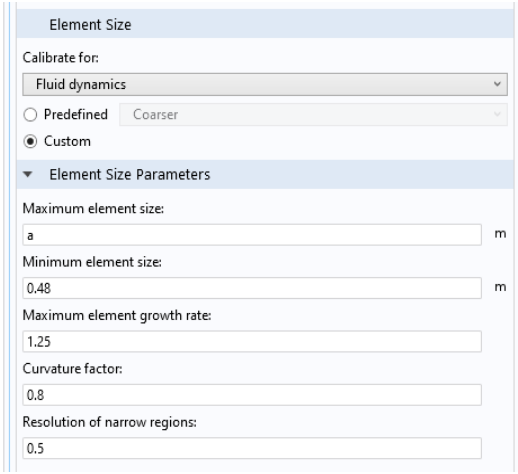

Fig.16. Variable **a** in the Maximum element size field

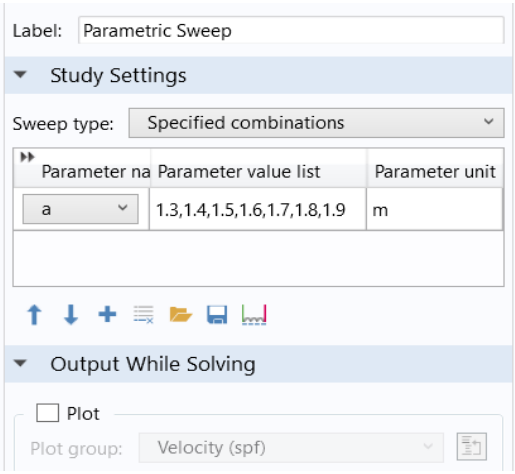

Fig.17. Seven Values of max element size

Software will calculate results for all seven grid densities. Results will be presented and compared with the results for two edge elements in the Laminar flow study: *Drivers cabin right edge*, shown in Fig.8.a and *Bucket edge* shown in Fig.8.b. Parameter to be compared is the pressure in these two parts of the Bucket Crane.

a)

a (m)	Pressure (Pa)
1.3000	185.20
1.4000	178.52
1.5000	178.72
1.6000	189.30
1.7000	188.75
1.8000	186.52
1.9000	185.99

b)

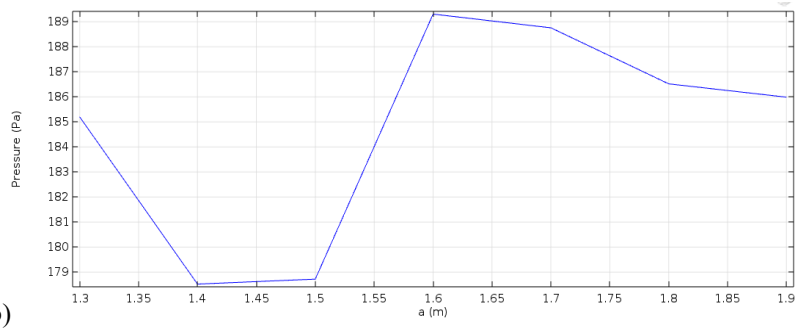

Fig.18. Results in (a) Table form and (b) Graphics of maximum values of Pressure for the Drivers cabin right edge for 7 types of grid densities

In Fig.18 are shown Table results and graphics of Pressure for the Cabin right edge for 7 values of elements sizes. In Fig.18.b, horizontal axes is the Grid density with maximum elements sizes (variable a), and in vertical axes is Pressure.

Referring to Fig. 8.a, in the graph for Cabin right edge, maximum pressure is $P_{cab} \approx 189\ Pa$. This is for the case of Coarser Mesh, that had *Maximum element size* of 1.56 m. The result on the table in Fig.18.a, for variable ***a*** values around 1.6 m is very close with the result of maximum Pressure $P_{cab} \approx 189\ Pa$. Based on the Graph in Fig.18.b, the values of Pressure variate around the value P ≈ *186 Pa,* and shows no divergence.

In Fig.19, are shown Table results and graphics of Pressure for the Bucket edge for 7 types of grid densities.

a)

a (m)	Pressure (Pa)
1.3000	137.69
1.4000	145.82
1.5000	145.34
1.6000	150.91
1.7000	146.92
1.8000	150.56
1.9000	147.00

b)

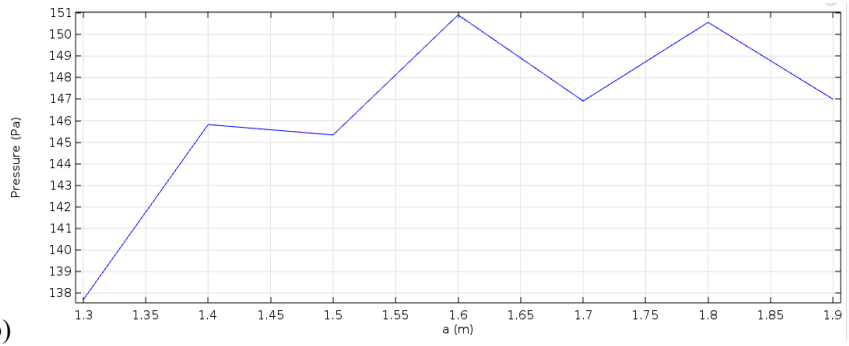

Fig.19. Results in (a) Table form and (b) Graphics of maximum values of Pressure of the Bucket edge for 7 types of grid densities

Referring to Fig. 8.b, in the graph for Bucket edge, maximum pressure is $P_{cab} \approx 147\ Pa$. This is also for the case of Coarser Mesh, that had *Maximum element size* of 1.56 m. This result is very close with the result of the maximal value of Pressure in Fig.19 for the values of variable ***a*** between 1.5 and 1.6 m. Based on the Graph in Fig.19.b, the values of Pressure variate around the value of $P \approx 147\ Pa$, which is the same value as in Fig.8.b, and shows no divergence.

As a summary, results of Grid Independence analysis shows minor differences for the results of Pressure for two parts of Bucket Crane presented in Fig.8 and they do not diverge, which gives the trust that results of analysis are accurate.

In the same way, Grid Independence analysis can be done for surfaces and volumes in the model, and compared with other CFD parameters presented above.

9. Conclusions

We examined the effects of side wind blowing on the bucket crane in this paper. According to the findings, when the side wind strikes the crane, it disperses unevenly, causing whirls and a vortex. This produces negative effects. The crane's structure is affected by the Side wind not only on its right side, but also on the bottom and on the back of the cabin. Another important result is that the crane is also affected on its right (outlet) side.

The wind velocity around the crane, compared to the inlet initial velocity $U_0 = 16.31$ *km/h* increases by roughly 38% in laminar flow and 44.7% in turbulent flow (Fig.5 & Fig.11). This is a concern for work safety while it can produce swinging and oscillations on the crane, especially on the elevated bucket where workers stand. In this case, the work with cranes should be halted. Results of the vorticity around the crane for both regimes show extreme whirls around the crane (Fig.6 & Fig.12). Results of other parameters, for both flow regimes are comparable and show turbulent distribution on and around the crane. The pressure and the total stress are intense on the lower parts of the crane. At the end, results are tested with Grid Independence analysis for accuracy.

Some types of bucket cranes usually have outriggers that can be applied to increase safety. Outriggers can improve safety on the lower part of the crane in the event of strong winds, but they are ineffective on the raised bucket where workers are standing. In this study, we showed that wind blow significantly affects the bucket, as best seen by the vorticity graphs.

Similar crane types, such as mobile cranes with telescoping booms, construction cranes, and shipyard cranes, can be analyzed using this methodology. It can be used for higher wind velocity in areas with strong winds.

REFERENCES

1 *Isuzu aerial plaftorm truck*, https://www.isuzutruckscn.com/isuzu-aerial-platform-truck_c28

2. *J. Huang, E. Maleki, W. Singhose*, Dynamics and swing control of mobile boom cranes subject to wind disturbances, IET Control Theory and Applications, ***v*ol. 7*(9)*,** 2013. doi: 10.1049/iet-cta.2012.0957.

3. *I. Doçi, Sh. Lajqi, G. Krasniqi*, Stability analysis of Tower crane during rotational motion and influence of wind, International Review of Mechanical Engineering, **vol. 12(11)**, 2018.

4. ISO 4302:2016, Cranes – Wind Load Assessment.

5. *Bucket Truck Tip Over: 6 Safety Tips*, https://hardhattraining.com/bucket-truck-tip-over/

6. *Vaughan J.*, Dynamics and control of mobile cranes, Thesis, Georgia Institute of Technology, 2008.

7. D. *Cekus, R. Gnatowska, P. Kwiato*, Impact of Wind on the Movement of the Load Carried by Rotary Crane, MDPI Journal Applied Sciences, **vol. 9 (18),** 2019; doi:10.3390/app9183842 .

8. *2019 Isuzu NRR Bucket Truck technical features*, https://www.mjtrucknation.com/2019-isuzu-nrr-bucket-truck/ ; https://www.youtube.com/watch?v=D-T4afs5Hv0.

9. *Comsol Multiphysics Help & User guide*, COMSOL Multiphysics®, v.5.1, www.comsol.com .

10. *Comsol Multiphysics CFD Module*, https://www.comsol.com/cfd-module.

11. *X. Zhang*, Crosswind stability of vehicles under nonstationary wind excitation, Dissertation, Karlsruher Institut für Technologie (KIT), April 2015.

12. *F. A. Monteiro, R. M. Moreira,* CFD Analysis of Wind Effects on Lifted Loads, International Journal of Advanced Engineering Research and Science (IJAERS), **vol. 6(11)**, 2019; https://dx.doi.org/10.22161/ijaers.611.

13. *I. Doçi, F. Shala,* Numerical analysis of the rear wind influence on the truck during travel, Strojnícky časopis – Journal of Mechanical Engineering, **vol. 72(2),** 2022.

14. F. *Frunzulica, A. Dumitrache, I-.C. Stan, M.-A. Lupescu*, Using CFD to Improve Vehicles Aerodynamics, Central European Symposium on Thermophysics (CEST) 2019.
15. *A. A. Estébanez, J.J. del Coz Díaz, F.P. Á. Rabanalb, P. P.l Muñoza, P.J. G. Nietoc*, Numerical investigation of truck aerodynamics on several classes of infrastructures, Wind and Structures, **vol. 26(1),** 2018.
16. *M. Augustyn, M. Barski*, Numerical and Analytical Estimation of the Wind Speed Causing Overturning of the Fast-Erecting Crane-Part II, Applied Sciences, **vol. 14/4694**, 2024. https://doi.org/10.3390/app14114694 .
17. *L. Kumar*, Design and analysis of two different modified trucks using CFD, International Journal of Civil Engineering and Technology, **vol. 8(7)**, 2017.
18. *S. Walczak*, Analysis of vehicle dynamics under sadden cross wind, Scientific Conference on Automotive Vehicles and Combustion Engines (KONMOT 2016); doi:10.1088/1757-899X/148/1/012030.
19. https://www.williamsugg.co.uk/height-of-street-lights/
20. https://heavyequipmentcollege.edu/wind-speed-guide-for-mobile-crane-operation/
21. *R. Isherwood, R. Richardson*, The effect of wind loading on the jib of a luffing tower crane, Health and Safety Laboratory, RR917 Research Report, HSE Books, 2012.
22. *E. J. Finnemore, J. B. Franzini*, Fluid Mechanics with Engineering Applications, 10th Edition, McGraw Hill , 2002.
23. *White, F. M*., Fluid mechanics, 7th ed., McGraw-Hill series in mechanical engineering, 2011.
24. *T. Cebeci, J.R. Shao, F. Kafyeke, E. Laurendeau*, Computational Fluid Dynamics for Engineers, Springer, 2005.
25. *Bihya Sun*, On the Reynolds-Averaged Navier-Stokes Equations, Cambridge University Press, 2001.
26. *Chemeurope.com*, "Reynolds-Averaged Navier–Stokes Equations", https://www.chemeurope.com/en/encyclopedia/Reynolds-averaged_Navier-Stokes_equations.html#_note-0/
27. https://proliftcrane.com/mobile-crane-safety-in-windy-conditions/
28. https://doc.comsol.com/5.5/doc/com.comsol.help.cfd/cfd_ug_fluidflow_single.06.093.html
29. https://www.comsol.com/support/knowledgebase/1261